An Implicit Controlling of Adaptive Neuro Fuzzy Inference System Controller for The Grid Connected Wind Driven PMSG System

Nirmal Kumar Agarwal [1], Manish Prateek[2], Neeta Singh [3], Abhinav Saxena [4*]

[1] SOES at G D Goenka University-Sohna, Gurugram (Haryana) 122103, India
[2] SOES at G D Goenka University-Sohna, Gurugram (Haryana) 122103, India
[3] USAR, Guru Gobind Singh Indraprastha University, (New Delhi) 110032, India
[4]Department of Electrical Engineering, JSS Academy of Technical Education, Noida
Emails: nirmalnitham@gmail.com;manish.prateek@gdgu.org; neeta.usar@ipu.ac.in; abhinaviitroorkee@gmail.com

Abstract

The article presents the design and control of the adaptive neuro fuzzy Inference system (ANFIS) for the wind-driven permanent magnet synchronous generator (PMSG) in the grid connected system. The rectifier and inverter are connected with the PMSG output and the grid for maintaining the voltage at the grid under variable wind operations. Such interconnections have many challenges, like high harmonics at the output and an improper voltage profile. The harmonics are measured in terms of total harmonic distortion (THD). Performance parameters like peak overshoot and settling time of DC link voltage and rotor speed have been measured. The control of the rectifier and inverter has been assessed with the ANFIS and PID controllers. A closed strategic mechanism has been developed for the ANFIS and PID controllers for improving the performance parameters and harmonics.. Finally, it is observed that the peak overshoot (%) and settling time (sec) of the DC link voltage with ANFIS are 5.2% and 2.9 sec, which are found to be less in comparison to the PID controller with the values of 6.1% and 3.8 sec and other existing methods. Similarly, the settling time (sec) of rotor speed with ANFIS is 1.1 sec, which is less than the settling time (2.6 sec) of the PID controller. Another advantage of ANFIS is the reduction of THD (%) of 5.1% with respect to THD (%) of PID controllers of 6.2% and other existing methods. The reduced THD shows the improved version of the voltage profile.

Keywords: PMSG; Wind; FLC; FO-PID; THD

1. Introduction

With the increasing demand for load, various generating units are planning to integrate with the grid. Especially renewable energy sources like wind, solar, etc. are connected to the existing grid to meet the excessive load power. In this article, a wind driven PMSG based system has been considered for optimal control of the output. In the papers [1–3], a nonlinear optimum control approach is designed for a wind energy generation system that includes a small wind turbine, a PMSG, a back-to-back power converter, and an LCL filter that is connected to the grid. The monitoring and handling of several system factors, such as generator angular speed, DC-link voltage, and reactive power, are the primary control goals in this energy system. For both the generator-side converter and the grid-side converter, the implementation of optimum controllers based on the state-dependent coefficient factoring technique is suggested in order to achieve these goals [1–3]. The proposed control strategy's benefits include a wide operating range for the system because the design of the controller considers the nonlinearities of the system, as well as effective trajectory tracking of time-varying references produced by a maximum power point tracking algorithm that makes use of a wind speed estimator. Additionally, an LCL filter is used to reduce the harmonic component of the current that is injected into the utility grid in order to comply with connection standards, which call for a THD below a specific threshold [4–5]. It is highly challenging to identify an impending stator.

Doi: https://doi.org/10.54216/FPA.120216
Received: January 25, 2023 Revised: April 28, 2023 Accepted: June 24, 2023

winding defect in a permanent magnet synchronous wind generator (PMSWG) because the variations in terminal electrical parameters caused by the fault are faint and erratic. In the winding of a PMSWG, this article models the beginnings of stator winding problems at various degrees of insulation degradation. It uses a co-simulation technique that combines a finite element model with external circuits. By examining the stator current, the Hilbert-Huang transformation is used to identify an interturn insulation problem at a relatively early stage. The minimal detectable severity degree of the interturn defect in this study is reduced, which is a lot better than the best record in the literature, according to detection results [6–10].

A sensor failure robust control strategy for PMSG-based direct drive wind energy conversion systems (WECSs) is presented in the articles [11–15]. Since such measurements are necessary to determine control actions for the power electrical Inferences in the WECSs, accurate measurement of WECS quantities, such as generator as well as grid-side currents, the generator velocity, and dc link voltage, is of utmost importance to guarantee the reliable and efficient operation of PMSG-based WECSs. Weak sensors that measure WECS quantities incorrectly can have a negative impact on the WECS's ability to operate effectively and consistently. Any error in the sensor measurements is regarded as a sensor error in these papers [11–15]. Over the past ten years, the offshore wind farm with PMSG as its foundation has developed quickly. Many nations have proposed specifications for the fault ride-through (FRT) in order to prevent the disconnecting of the offshore wind farms during a fault. conventional FRT strategy. The safety of the PMSG will also be impacted since the chopper circuit for the PMSG needs to consume all of the mismatching energy and the impulse current is too large during the fault. In this study, the superconducting fault current limiter (SFCL) is used to improve the FRT's functionality in an offshore wind farm based on PMSG. In the suggested concept, the resistive SFCL can lower the use of energy and enhance the hopper loop's functionality by collecting the grid-side converter's (GCS) power during the malfunction. The comparison simulation results demonstrate that the suggested plan is workable [16–20]. Cyber-physical systems that are human-centered, decentralized, and highly automated have been discussed [21]. [22] provides a discussion of the effective implementation of deep Q-routing in opportunistic networks. Residual Variational Autoencoder-Based Effective Video Anomaly Detection has been explored in [23].

The proposed model does not include any type of filter to reduce the level of harmonics, or THD (%). Such a benefit has been achieved with the involvement of the adaptive neuro fuzzy Inference system(ANFIS) for the control of converters, while uniform and non-uniform filters are needed in models involving fusion optimization techniques [24]. The fusion process techniques [25] also involve a lot of complexity, while the proposed model has very reduced complexity.

By doing the exhaustive survey, a lot of challenges and quantifiable information have come out. It is observed that a lot of distortion or harmonics at the grid output are attained with the existing methods. In addition to this, peak overshoot and settling times of performance parameters are quite high with the existing techniques. In order to overcome such issues, ANFIS has been implemented to reduce the THD (%) of the output voltage. In addition to this, peak overshoot (%) and settling time (sec) of dc link voltage and rotor speed have to be controlled with the ANFIS controller. It is observed that the most reduced THD (%) of the grid voltage is attained with the ANFIS controller in comparison to the PID controller and other existing techniques. The reduced THD (%) ensures an improved version of the output voltage. Further, minimum peak overshoot (%) and settling time (sec) of dc link voltage and rotor speed are attained with the ANFIS controller in comparison to the PID controller and existing techniques.

2. Mathematical modeling of PMSG

The PMSG is used as the study's wind turbine generator because of the permanent magnet's ability to self-excite, which eliminates excitation loss, or because excitation loss does not increase as the number of poles doubles. Using a two phase synchronous reference rotating frame (d-q frame), where the q-axis is 90° ahead of the rotational axis, the dynamical representation of the d-axis with PMSG is constructed. The electrical model of a PMSG is represented by the differential equations from Eq. 1 to Eq. 3 in a synchronous reference rotating frame.

$$\frac{d(i_d)}{dt} = -\frac{r_a i_d}{L_d} + \omega_e \frac{r_a L_q}{L_d} i_q + \frac{U_d}{L_d} \tag{1}$$

$$\frac{d(i_q)}{dt} = -\frac{r_a i_q}{L_q} - \omega_e \left(\frac{L_q}{L_d} i_d + \frac{\lambda_o}{L_d}\right) + \frac{U_q}{L_q} \tag{2}$$

$$T_e = 1.5P((L_d - L_q) i_d i_q + i_q \lambda_o) \tag{3}$$

Where $\omega_e = P\omega_g$

where ra is the stator winding resistance, ωe and ωg are rotating speed in electrical and mechanical degree, λ◦ is flux generated, P is pole pair number, Ud and Uq are d and q axis voltages, Ld and Lq are the inductances in d and q axis, Te is electromagnetic torque. The general diagram of wind driven PMSG is shown in Fig.1

Doi: https://doi.org/10.54216/FPA.120216
Received: January 25, 2023 Revised: April 28, 2023 Accepted: June 24, 2023

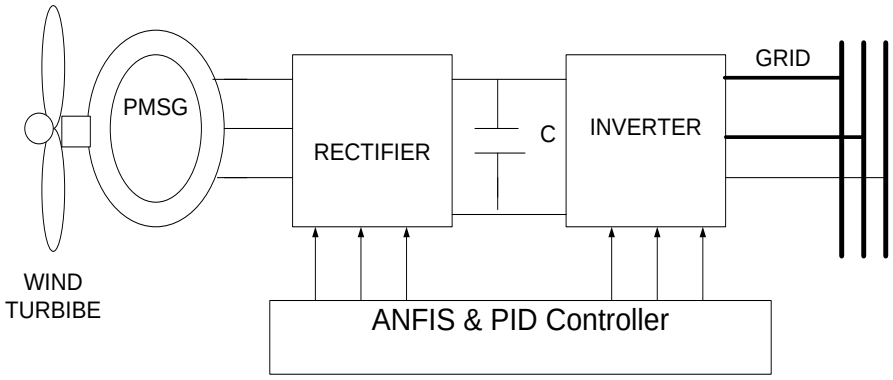

Figure 1: Wind driven PMSG based converters

3. Maximum power extraction from wind turbine

In order to generate enough power, the wind turbine is operated at its maximum capacity. Power coefficient (Cp) affects the amount of power (P) that can be generated by a wind turbine. The tip to speed ratio (TSR) and pitch angle (β) both affect the power coefficients. By maximizing the power coefficient, the peak power must be attained. Eq. 4 provides the expression for the power coefficient.

$$C_p(\lambda,\beta) = \lambda^{2.1}\beta^{1.6} + \beta^{3.2}e^{\lambda^{2.9}} + \lambda^{3.6}\beta^{3.1} \quad (4)$$

Generally, the power coefficient is given by the ratio of output delivered power to generated power from wind turbine as shown in Eq.5

$C_p(\lambda,\beta)$ = Power delivered /Power generated (5)

The variation of the turbine output power with turbine speed for the various wind speed and different pitch angle is shown in Fig.2.

The maximum power is attained at maximum wind speed of 12 m/s for pitch angle of 0 degree.

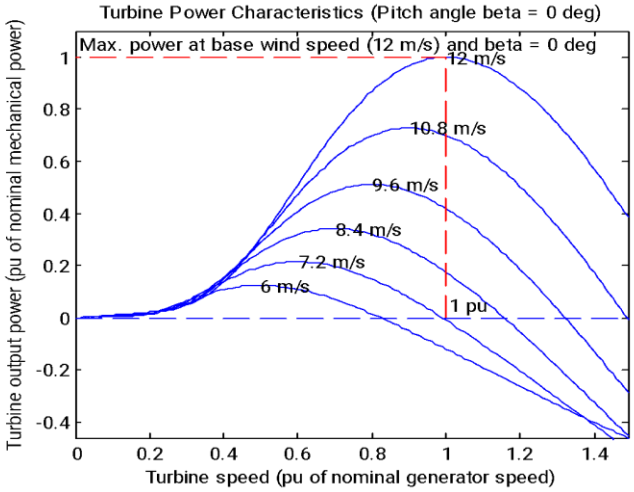

Figure 2: Variation of turbine output power with turbine speed

4. Design of rectifier and inverter using PID controller

The design of connected converters like rectifier and inverter between wind driven PMSG and the grid using PID controller has been discussed here. The design of each converter using PID controller has been described as :

A) Inverter design using PID controller

It begins with the measurement of three phase current (I_{abc}) and three phase voltage (V_{abc}). The conversion of three phase components (abc) has been converted into two axis coordinates (dqo) with the help of Clarke and park transformation. The q-component of current is compared with its reference value which further passes through PI controller and gives the measured q-component of grid voltage which is given in Eq.6

$$(I_q - I_q^*)(k_p + \frac{k_i}{s} + sk_d) = V_{gq}^* \quad (6)$$

Doi: https://doi.org/10.54216/FPA.120216
Received: January 25, 2023 Revised: April 28, 2023 Accepted: June 24, 2023

The measured q-component is added with actual q-component of grid voltage which gives reference voltage as shown in Eq.7

$$V_{gq}^{*} + V_{gq} = V_{gq}^{ref} \tag{7}$$

Now, the measured value of DC voltage is compared with its reference value and its output passes through PID controller which gives the error as given in Eq.8

$$(800 - V_{dc})(k_{p1} + \frac{k_{i1}}{s} + sk_{d1}) = e \tag{8}$$

Further this error is compared with its reference value of direct current and passes through PID controller which gives the d-axis grid voltage as given in Eq.9

$$(e\text{-}I_{d}^{*})(k_{p2} + \frac{k_{i2}}{s} + sk_{d2}) + V_{gq} = V_{gd}^{*} \tag{9}$$

The measured d-component is added with actual d-component of grid voltage which gives reference voltage as shown in Eq.10

$$V_{gd}^{*} + V_{gd} = V_{gd}^{ref} \tag{10}$$

Now $V_{g,dq}$ will be converted into Vabc with the help of inverse Clarke and inverse park transformation. The Vabc will be given as reference signal to PWM converter for generating the pulses to switch ON the inverter. The process of controlling the inverter using PID controller is shown in Fig.3

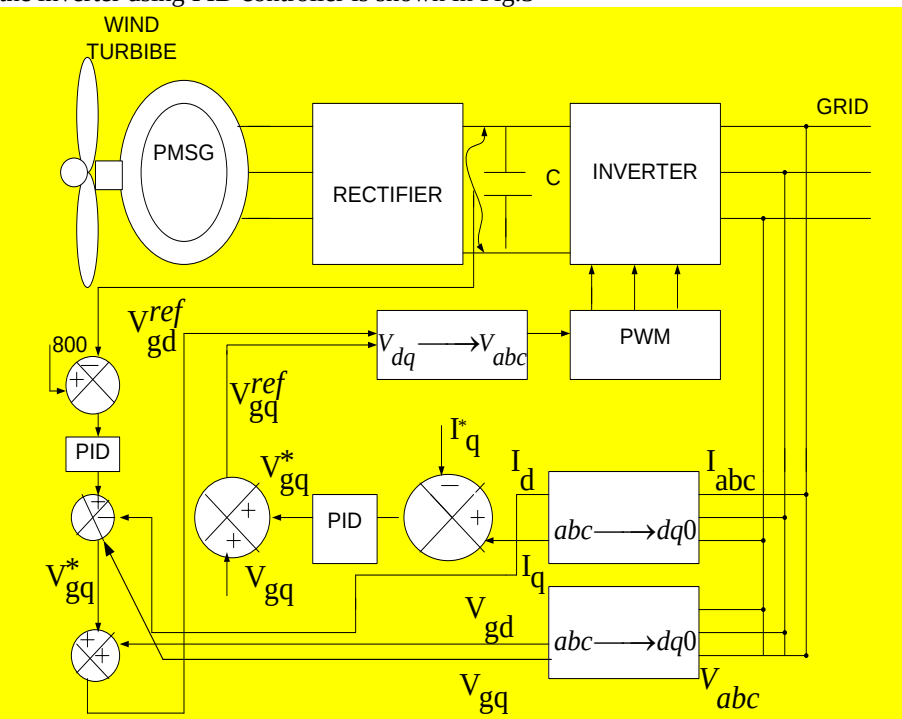

Figure 3: controlling of inverter using PID controller

B) Rectifier design using PID controller

The reactive power measured from the wind turbine is compared with its reference value and this difference pass through PID controller which gives the reference value of q-component of rotor current as shown in Eq.11

$$(Q_{s}\text{-}Q_{s}^{*})(k_{p3} + \frac{k_{i3}}{s} + sk_{d3}) = I_{rq}^{*} \tag{11}$$

The measured and reference value of q-component of rotor current is compared and its output passes through PID controller which gives q-axis of voltage as mentioned in Eq.12

$$(I_{rq}^{*} - I_{rq})(k_{p4} + \frac{k_{i4}}{s} + sk_{d4}) = V_{q} \tag{12}$$

The ratio of wind speed(V) and tip to speed ratio (TSR) to the radius of the blade is known as reference rotor speed as given in Eq.13

$$\omega_{r}^{*} = \frac{V\lambda}{R} \tag{13}$$

Doi: https://doi.org/10.54216/FPA.120216
Received: January 25, 2023 Revised: April 28, 2023 Accepted: June 24, 2023

This reference rotor speed is compared with measured rotor speed and further passes through PID controller which gives the real power as shown in Eq.14

$$(\omega_r^* - \omega_r)(k_{p6} + \frac{k_{i6}}{s} + sk_{d6}) = P \quad (14)$$

The real power is further divided by reference value of d-component of current which further gives measured value of d-component of current as mentioned in Eq.15

$$\frac{P}{I_{rd}^*} = I_{rd} \quad (15)$$

This reference and actual value of current is compared and passes through PID controller which gives d-component of voltage as mentioned in Eq.16

$$(I_{rd}^* - I_{rd})(k_{p7} + \frac{k_{i7}}{s} + sk_{d7}) = V_d \quad (16)$$

Now V_{dq} will be converted into Vabc with the help of inverse Clarke and inverse park transformation. The Vabc will be given as reference signal to PWM converter for generating the pulses to switch ON and OFF the inverter. The process of controlling the rectifier using PID controller is shown in Fig.4

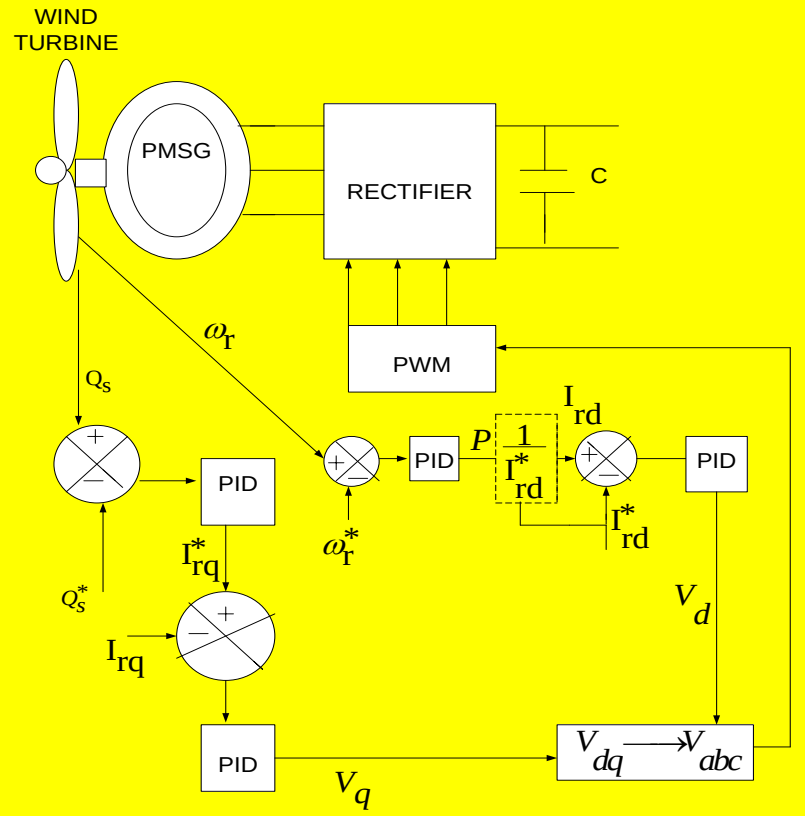

Figure 4: Controlling of rectifier using PID controller

5. Design of rectifier and inverter with ANFIS

The design of connected converters like rectifier and inverter between wind driven PMSG and the grid using ANFIS has been discussed here. The design of each converter using ANFIS has been described as:

A) Inverter design using ANFIS

Design of ANFIS for the inverter controlling begins with the output of Eq.5 which is given as error(e), after this one more input has been considered which termed as change in error (Δe) as shown in Eq.17

$$\Delta e = e(t) - e(t-1) \quad (17)$$

Let's consider e=e1 and $\Delta e = e_2$

The output Vgd* can be expressed in terms of inputs as given in Eq.18

Doi: https://doi.org/10.54216/FPA.120216
Received: January 25, 2023 Revised: April 28, 2023 Accepted: June 24, 2023

$$V_{gd}^{*}=e_1\ln(e_2)+e_2\ln(e_1) \quad (18)$$

Now the Eq.18 can be expressed as general form of ANN as in Eq.19

$$Y_1=X_1W_1+X_2W_2 \quad (19)$$

$$Y_1=V_{gd}^{*},\ X_1=e_1,\ W_1=\ln(e_2),\ X_2=e_2,\ W_2=\ln(e_1)$$

Now these weights are trained with the help of fuzzy logic controller. The ANFIS structure for the controlling of inverter is shown in Fig.5

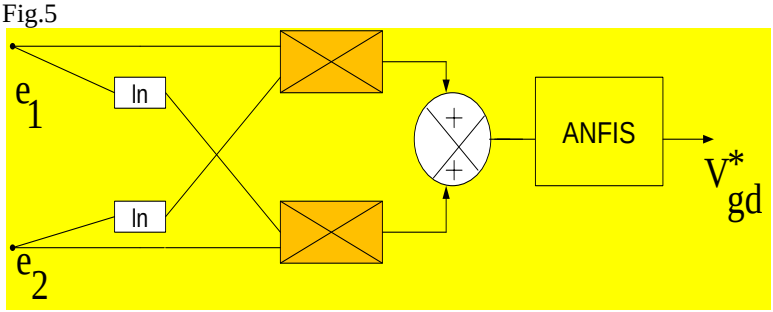

Figure 5: ANFIS Structure for inverter controlling

The mathematical representation of the membership function in triangular manner is shown in Eq.20 and Eq.21.The rules of ANFIS is shown in Fig.6. The mapping between the rules of the inputs and output is shown in Table.1

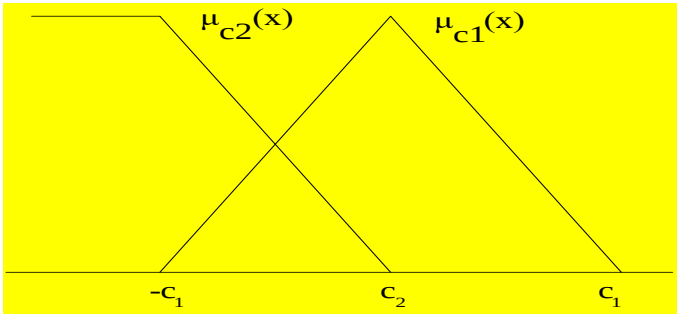

Fig.6 Fuzzy rules of ANFIS for inverter

$$\mu_{c1}=\begin{cases}1, X\le -c_1\\ \dfrac{X-c_2}{-c_1-c_2}, -c_1<X<c_2\\ 0, X>c_2\end{cases} \quad (20)$$

$$\mu_{c2}=\begin{cases}1-\dfrac{X-c_2}{c_1}, |X-c_2|\le c_1\\ 0, |X-c_2|\ge c_1\end{cases} \quad (21)$$

where the value of c_1, c_2 are managed in order to minimize the error.

Table1: Mapping between inputs and output for inverter controlling

Rules	**NB**	**NS**	**ZZ**	**PS**	**PB**
NB	PB	PS	NB	PB	NB
NS	NS	NS	ZZ	PB	PB
ZZ	ZZ	NS	ZZ	ZZ	ZZ
PS	PS	NS	ZZ	PS	PB
PB	NS	NB	ZZ	ZZ	PB

The output of FLC is V_{gd}^{*} and process of inverter controlling using ANFIS is shown in Fig.7

Doi: https://doi.org/10.54216/FPA.120216
Received: January 25, 2023 Revised: April 28, 2023 Accepted: June 24, 2023

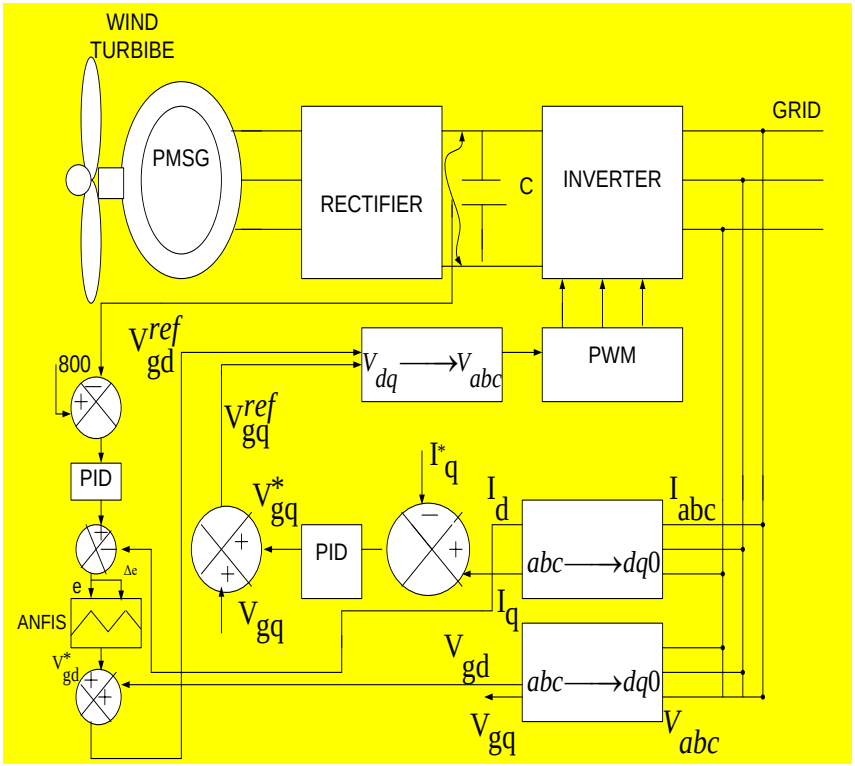

Figure 7: Controlling of inverter using ANFIS

B) Rectifier controlling and design using ANFIS

The controlling of the rectifier using ANFIS begins with the Eq.11 in which difference between reference and measured speed is considered as error (e1) as expressed in Eq.22

$$e = \omega_r^* - \omega_r = e_3 \tag{22}$$

Now another can be considered as rate of change in error which is expressed in Eq.23.

Rate of change of error = $\frac{de_1}{dt} = e_4$ (23)

The output Vgd* can be expressed in terms of inputs as given in Eq.24

$$V_{gd}^* = e_3 E^{e_4} + e_4 E^{e_3} \tag{24}$$

Where E is exponential form

Now the Eq.22 can be expressed as general form of ANN as in Eq.25

$$Y_1 = X_1 W_1 + X_2 W_2 \tag{25}$$

$$Y_1 = V_{gd}^*,\ X_1 = e_3,\ W_1 = E^4,\ X_2 = e_4,\ W_2 = E^3$$

Now these weights are trained with the help of fuzzy logic controller.

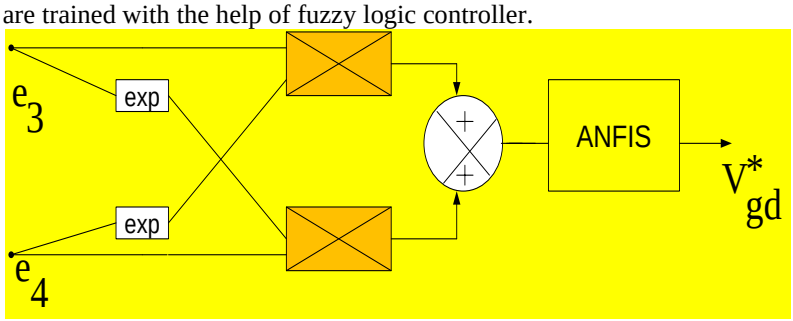

Figure 8: ANFIS Structure for rectifier controlling

Doi: https://doi.org/10.54216/FPA.120216
Received: January 25, 2023 Revised: April 28, 2023 Accepted: June 24, 2023

The ANFIS structure for the controlling of rectifier is shown in Fig.8 while fuzzy rules of ANFIS is shown in Fig.9.The mathematical representation of the membership function in triangular manner is shown in Eq.26 and Eq.27

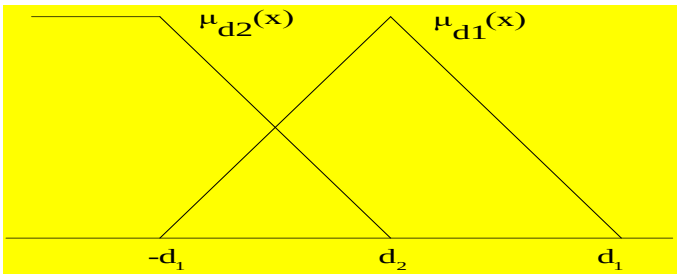

Figure 9: Fuzzy rules of ANFIS for rectifier

$$\mu_{d1}=\begin{cases}1, X \le -d_1 \\ \dfrac{X-d_2}{-d_1-d_2}, -d_1 < X < d_2 \\ 0, X > d_2\end{cases} \quad (26)$$

$$\mu_{d2}=\begin{cases}1-\dfrac{X-d_2}{d_1}, |X-d_2| \le d_1 \\ 0, |X-d_2| \ge d_1\end{cases} \quad (27)$$

where the value of d_1, d_2 are managed in order to minimize the error. The output of ANFIS is real power(P) and process of rectifier controlling is shown in Fig.10

The two inputs of the ANFIS with triangular membership function are mapped each other with 5x5 fuzzy rule as given in Table.2.

Table 2: Mapping between inputs and output for rectifier controlling

Rules	**NB**	**NS**	**ZZ**	**PS**	**PB**
NB	PB	PS	NB	NS	PB
NS	PB	PS	ZZ	NS	NB
ZZ	ZZ	ZZ	ZZ	ZZ	ZZ
PS	NB	NS	ZZ	PS	PB
PB	PB	PB	ZZ	PB	PS

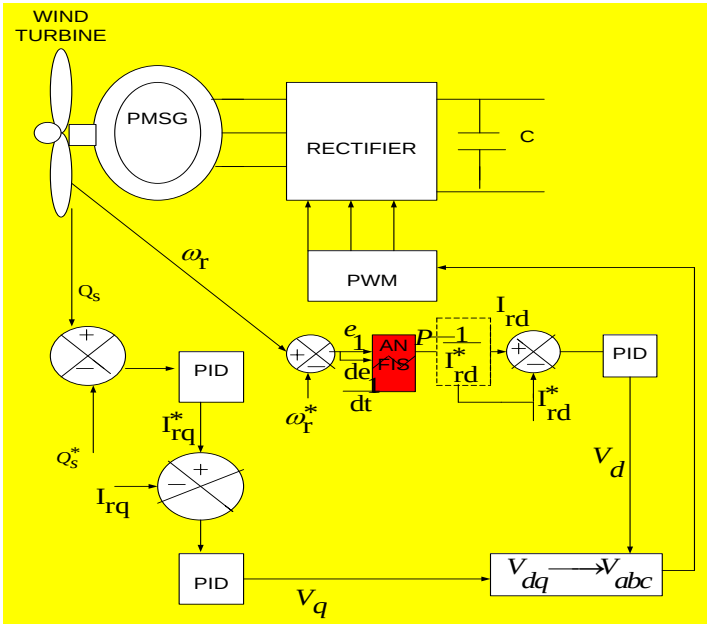

Figure 10: controlling of rectifier using ANFIS

Doi: https://doi.org/10.54216/FPA.120216
Received: January 25, 2023 Revised: April 28, 2023 Accepted: June 24, 2023

After the implementation of fuzzy rules between inputs and output, various performance parameters have been measured which will be discussed in the next section.

6. Result and discussion/ Performance parameter analysis with PID and ANFIS controller

The design of PID controllers and ANFIS for inverter and rectifier control has been discussed in sections IV and V. In this section, various performance parameters like voltage across the DC link, speed of the rotor, etc. have been measured.

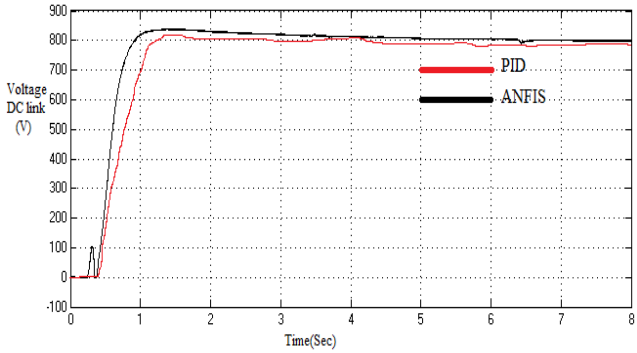

Figure 11: Voltage across DC link using PID and ANFIS

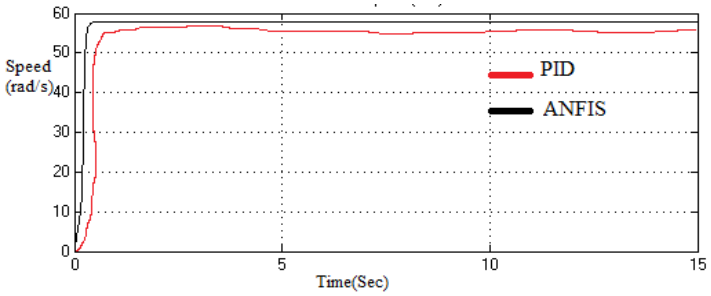

Figure 12: Rotor speed of PMSG using PID & ANFIS

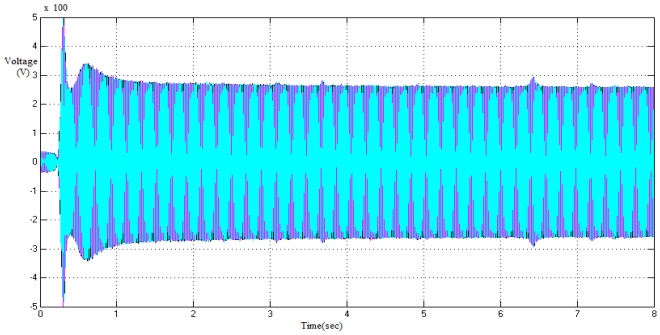

Figure 13: Three phase voltage across the grid using ANFIS

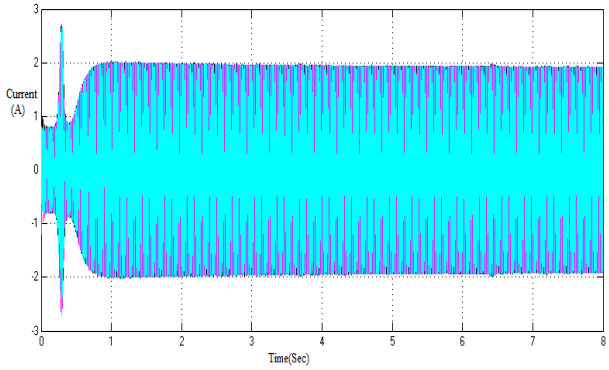

Figure 14: Three phase current across the grid using ANFIS

Doi: https://doi.org/10.54216/FPA.120216
Received: January 25, 2023 Revised: April 28, 2023 Accepted: June 24, 2023

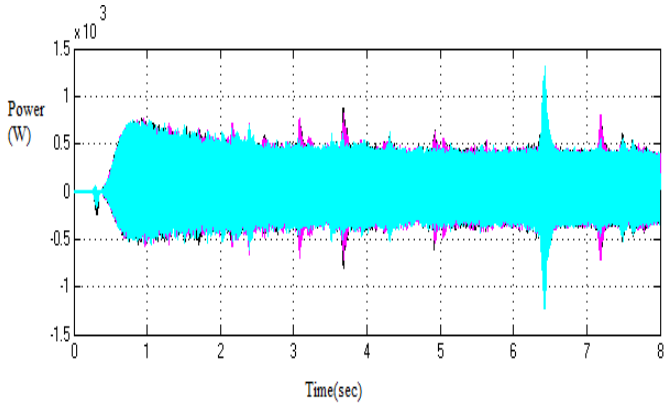

Figure 15: Real power flow in the grid using ANFIS

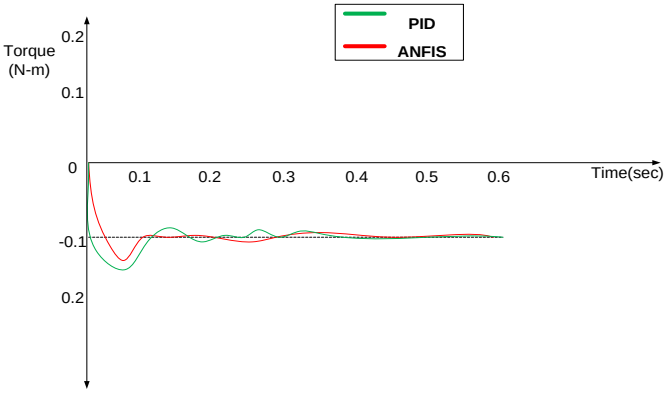

Figure 16: Torque of the PMSG using ANFIS and PID

The voltage across the DC link is measured using ANFIS and PID controllers, as shown in Fig. 11. It is observed that peak overshoot (5.2%%) and settling time (2.9 sec) of DC link voltage are found to be less with ANFIS in comparison to PID controllers, with values of 6.1% and 3.8 sec, respectively. The ANFIS also shows better results in comparison to existing methods [14], [16]. Similarly, the speed characteristics of PMSG have been plotted for these three controllers as shown in Fig. 12, which further shows the dominance of ANFIS over PID controllers for estimating the settling time (1.1 sec and 2.6 sec, respectively to attain its steady state.
Further, three phase voltage and current are measured across the grid using ANFIS due to its dominance, as shown in Figs. 13 and 14. In the same way, real power transferred to the grid using ANFIS is shown in Fig. 15. As the best speed performance is achieved with ANFIS, torque characteristics have been plotted using ANFIS, which shows the least peak overshoot and settling time with respect to the PID controller, as shown in Fig. 16. Now the comparative analysis of peak overshoot and settling time of DC link voltage using ANFIS, PID controller, and existing methods [14], [16] is shown in Table 3, and its graphical analysis is shown in Fig. 17.

Table 3: Peak overshoot and settling time of DC link voltage comparison with various method

Parameters	ANFIS	PID	Ref. [14]	Ref. [16]
Peak overshoot (%) of DC link voltage	5.2	6.1	7.1	7.7
Settling time(sec) of DC link voltage	2.9	3.8	4.4	4.8

Table 4 :Settling time of rotor speed comparison with various method

Parameters	ANFIS	PID	Ref. [14]	Ref. [16]
Settling time(sec) of rotor speed	1.1	2.6	4.9	5.1

Table 5: THD (%) of three phase voltage comparisons with various method

Parameters	ANFIS	PID	Ref. [14]	Ref. [16]
THD (%) of three phase voltage	5.1	6.2	7.1	7.7

Doi: https://doi.org/10.54216/FPA.120216
Received: January 25, 2023 Revised: April 28, 2023 Accepted: June 24, 2023

Table 6: Peak overshoot and settling time of torque comparisons with various methods

Parameters	ANFIS	PID	Ref. [14]	Ref. [16]
Peak overshoot (%) of torque	1.2	5.1	6.9	7.2
Settling time(sec) of torque	0.1	0.2	1.2	1.6

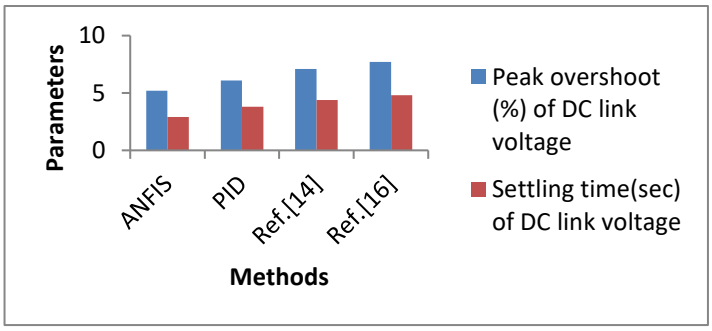

Figure 17: Graphical comparison of peak overshoot (%) and settling time(sec) of the DC link voltage with various methods

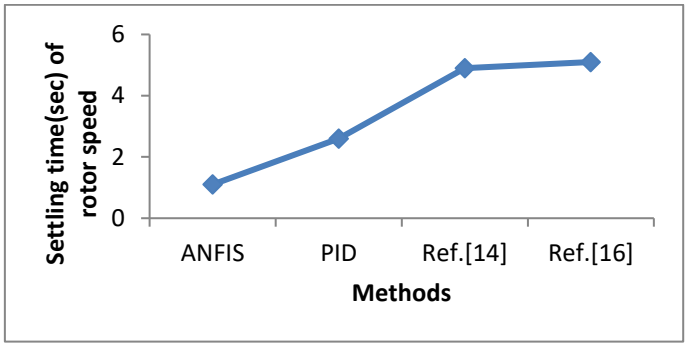

Figure 18: Graphical comparison of settling time(sec) of rotor speed with various methods

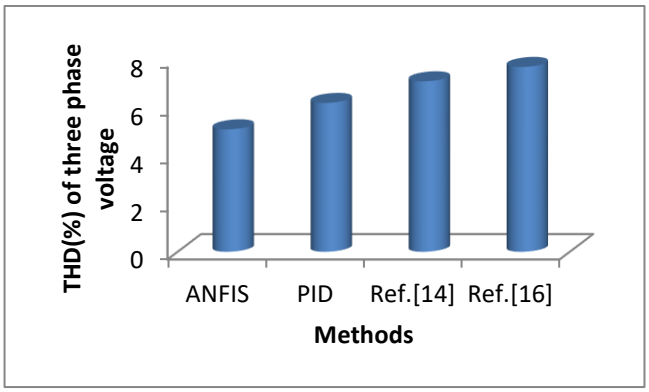

Figure 19: Graphical comparison of THD (%) of three phase voltage with various methods

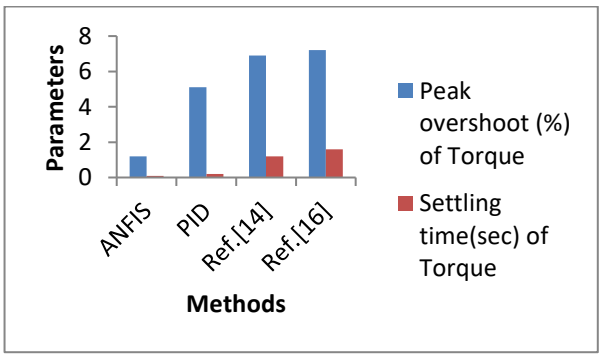

Figure 20: Graphical comparison of peak overshoot (%) and settling time(sec) of torque with various methods

Doi: https://doi.org/10.54216/FPA.120216
Received: January 25, 2023 Revised: April 28, 2023 Accepted: June 24, 2023

The comparison of peak overshoot (%) and settling time (sec) of the DC link voltage using ANFIS, PID, and existing methods (Ref. [14], [16]) has been shown in Table 3, and its graphical comparison is shown in Fig. 17. It is observed that the least overshoot and reduced settling time have been attained with ANFIS in comparison to other and existing methods.
In a similar way, the comparison of the settling time (sec) of the rotor speed of 1.1 sec using ANFIS is quite lesser than PID (2.6 sec), and existing methods (Ref. [14], [16]) have been shown in Table. 4, and their graphical comparison is shown in Fig. 18. It is again observed that the minimum settling time has been attained with ANFIS in comparison to other and existing methods. A similar kind of ANFIS dominance is achieved for torque in terms of reduced peak overshoot and less settling time, as shown in Table 6, and its graphical comparison is shown in Fig. 20.
At the end, in order to ensure power quality issues at the grid terminal, distortion, or harmonics, are measured in the form of total harmonic distortion (THD). Further, THD (%) of the three-phase voltage has been measured with ANFIS, PID, and existing methods (Ref. [14], Ref. [16]), as shown in Table 5, and its graphical comparison is shown in Fig. 19. It is further observed that a reduced THD (%) of 5.1% is attained with ANFIS in comparison to PID controllers with a value of 6.2%. Reduced THD (%) of the three-phase voltage indicates that the best voltage profile is attained with ANFIS in comparison to other methods. It is finally concluded that ANFIS gives more profound results in comparison to PID controllers and existing methods.

7. Conclusion

The adaptive neural fuzzy Inference system (ANFIS) for the grid-connected system's wind-driven permanent magnet synchronous generator (PMSG) is designed and controlled in the article. The grid and PMSG output are coupled with the rectifier and inverter. Such connections face a number of difficulties, including incorrect voltage profiles and excessive harmonics at the output. Total harmonic distortion (THD), a measure of harmonics, is used. Peak overshoot, settling time, and rotor speed of the DC link voltage are examples of performance parameters that have been measured. With the help of an ANFIS and PID controller, the control of a rectifier and an inverter has been evaluated. For the purpose of enhancing the performance parameters and harmonics, a closed strategic mechanism has been designed for the ANFIS and PID controllers. Finally, it is noted that, when compared to PID controllers and other existing methods, ANFIS is found to have the least amount of peak overshoot (%) and settling time (sec) for the rotor speed and DC link voltage. The decrease in THD (%) compared to PID controllers and other existing approaches demonstrates a further benefit of ANFIS. The voltage profile has been improved, as evidenced by the lower THD.

Funding: "This research received no external funding"

Conflicts of Interest: "The authors declare no conflict of interest."

References

[1] David Cortes-Vega; Fernando Ornelas-Tellez; Juan Anzurez-Marin,Nonlinear Optimal Control for PMSG-Based Wind Energy Conversion Systems, IEEE Latin America Transactions, Vol.19, Issue.7, pp. 1191 – 1198,July 2021
[2] Kaiqin Peng, Anqi He, Transient Stability Assessment of Power System with PMSG Involved, IEEE International Conference on Advances in Electrical Engineering and Computer Applications,vol.1, pp.753-756, 2022.
[3] Carlos Andres Ramos-Paja, Elkin Edilberto Henao-Bravo, Andres Julian Saavedra-Montes, MPPT Solution for Commercial Small Wind Generation Systems with Grid Connection, Energies, vol.16, no.2, pp.719, 2023.
[4] Huaren Wu,Coordinated Control of an Islanded Microintegrated Energy System with an Electrolyzer and Micro-Gas Turbine, International Journal of Photoenergy, vol.2022, no. 6195807, 2022.
[5] Jianhang Qian, Zhijie Liu, Ke-Jun Li, Liangzi Li, ZhongLin Guo,Reducing Submodule Capacitance for Modular Multilevel Converter-Based Medium-Voltage Wind Power Converter, Frontiers in Energy Research, vol.10, 2022
[6] Wang, C., Liu, X., & Chen, Z,Incipient Stator Insulation Fault Detection of Permanent Magnet Synchronous Wind Generators Based on Hilbert–Huang Transformation,IEEE Transactions on Magnetics, vol.50, no.11, pp. 1–4,2014
[7] J. Arellano-Padilla, M. Sumner, and C. Gerada,Winding condition monitoring scheme for a permanent magnet machine using highfrequency injection, IET Elect. Power Appl., vol. 5, no. 1, pp. 89–99, Jan. 2011.
[8] K. H. Kim,Simple online fault detecting scheme for short-circuited turn in a PMSM through current harmonic monitoring,IEEE Trans.Ind. Electron., vol. 58, no. 6, pp. 2565–2568, Jun. 2011.

Doi: https://doi.org/10.54216/FPA.120216
Received: January 25, 2023 Revised: April 28, 2023 Accepted: June 24, 2023

[9] N. Leboeuf, T. Boileau, B. Nahid-Mobarakeh, N. Takorabet, F. Meibody-Tabar, and G. Clerc, Inductance calculations in permanent magnet motors under fault conditions,IEEE Trans. Magn., vol. 48, no. 10, pp. 2605–2616, Oct. 2012..
[10] N. Leboeuf, T. Boileau, B. Nahid-Mobarakeh, N. Takorabet, F. Meibody-Tabar, and G. Clerc, Estimating permanent-magnet motor parameters under inter-turn fault conditions,IEEE Trans. Magn.,vol. 48, no. 2, pp. 963–966, Feb. 2012.
[11] S. Saha, M. E. Haque, C. P. Tan, and M. A. Mahmud,Sensor Fault Resilient Operation of Permanent Magnet Synchronous Generator Based Wind Energy Conversion System, vol.55, no. 4,pp. 4298 – 4308, 2019
[12] N. R. Ullah, K. Bhattacharya and T. Thiringer, Wind farms as reactive power ancillary service providers—Technical and economic issues, IEEE Trans. Energy Convers., vol. 24, no. 3, pp. 661-672, Sep. 2009.
[13] E. Prieto-Araujo, A. Junyent-Ferre, D. Lavernia-Ferrer and O. Gomis-Bellmunt,Decentralized control of a nine–phase permanent magnet generator for offshore wind turbines, IEEE Trans. Energy Convers., vol. 30, no. 3, pp. 1103-1112, Sep. 2015.
[14] V. Yaramasu and B. Wu, Predictive control of a three–level boost converter and an NPC inverter for high–power PMSG–based medium voltage wind energy conversion systems, IEEE Trans. Power Electron., vol. 29, no. 10, pp. 5308-5322, Oct. 2014.
[15] H. H. Alhelou, M. H. Golshan and J. Askari-Marnani, Robust sensor fault detection and isolation scheme for interconnected smart power systems in presence of RER and EVs using unknown input observer, Int. J. Elect. Power Energy Syst., vol. 99, pp. 682-694, 2018.
[16] Yaru Sheng,Chao Li,Hanru Jia,Bin Liu,Bin Li,Tim A. Coombs, Investigation on FRT Capability of PMSG-Based Offshore Wind Farm Using the SFCL, IEEE Transactions on Applied Superconductivity, vol.31, no.8, November 2021
[17] R. Li, L. Yu and L. Xu, Offshore AC fault protection of diode rectifier unit-based HVDC system for wind energy transmission, IEEE Trans. Ind. Electron., vol. 66, no. 7, pp. 5289-5299, Jul. 2019.
[18] R. Basak, G. Bhuvaneswari and R. Rahul, Low voltage ride-through of a synchronous generator based variable speed grid-Inferenced wind energy conversion system, IEEE Trans. Ind. Appl., vol. 56, no. 1, pp. 752-762, Oct. 2019.
[19] B. Xiang, Jinhui Luo, Lei Gao, Zhiyuan Liu, Yingsan Geng, Jianhua Wang, Satoru Yanabu Study on the parameter requirements for resistive-type superconducting fault current limiters combined with mechanical DC circuit breakers in hybrid AC/DC transmission grids, IEEE Trans. Power Del., vol. 35, no. 6, pp. 2865-2875, Dec. 2020.
[20] B. Li, C. Li and F. Guo, Application studies on the active SISFCL in electric transmission system and its impact on line distance protection, IEEE Trans. Appl. Superconductor, vol. 25, no. 2, Apr. 2015
[21] Manju Khari, Rubén González Crespo, Guest editorial of the special issue 'human-centric, decentralised, and hyper automated cyber-physical systems, Journal of Control and Decision, vol.10.no.1, pp. 1-2,2023.
[22] Manju Khari, Renu Dalal, Efficacious implementation of deep Q-routing in opportunistic network, Soft Comput, vol.27, pp.9459–9477 ,2023.
[23] Manju Khari, Ankit Kumar, Efficient Video Anomaly Detection using Residual Variational Autoencoder, International Conference on Communication System, Computing and IT Applications, Mumbai, India, pp. 50-55,2023
[24] Mohamed Saber, Pushan K. Dutta,' Uniform and Nonuniform Filter Banks Design Based on Fusion Optimization', Fusion: Practice and Applications, vol. 09, no. 01. pp. 29-37, 2022
[25] Omar Saad Ahmed, Fay Fadhil, Laith H. Jasim Alzubaidi, Riyadh Al-Obaidi,' Fusion Processing Techniques and Bio-inspired Algorithm for ECommunication and Knowledge Transfer', Fusion: Practice and Applications, Vol. 10, No. 01.pp. 143-155, 2023

Doi: https://doi.org/10.54216/FPA.120216
Received: January 25, 2023 Revised: April 28, 2023 Accepted: June 24, 2023